High-spin level structure in ^{94,95}Mo

Y. H. Zhang,[1] M. Hasegawa,[1] W. T. Guo,[1] M. L. Liu,[1] X. H. Zhou,[1] G. de Angelis,[2,3] T. M. Axiotis,[2] A. Gadea,[2] N. Marginean,[2] Martinez,[2] D. R. Napoli,[2] C. Rusu,[2] Zs. Podolyak,[4] C. Ur,[5] D. Bazzacco,[5] F. Brandolini,[5] S. Lunardi,[5] S. M. Lenzi,[5] R. Menegazzo,[5] R. Schwengner,[6] A. Gargano,[7] W. von Oertzen,[3,8] and S. Tazaki[9]

[1]*Institute of Modern Physics, Chinese Academy of Sciences, Lanzhou, China*
[2]*Istituto Nazionale di Fisisca Nucleare, Laboratori Nazionali di Legnaro, Legnaro, Italy*
[3]*Hahn-Meitner-Institut, Berlin, Germany*
[4]*Department of Physics, University of Surrey, Guildford GU2 7XH, United Kingdom*
[5]*Dipartimento di Fisica dell'Universitá and Istituto Nazionale di Fisica Nucleare, Sezione di Padova, Padova, Italy*
[6]*Institut für Kern-und Hadronenphysik, Forschungszentrum Rossendorf, Dresden, Germany*
[7]*Istituto Nazionale di Fisica Nucleare, Sezione di Napoli, Napoli, Italy*
[8]*Freie Universität Berlin, Fachbereich Physik, Berlin, Germany*
[9]*Department of Applied Physics, Fukuoka University, Fukuoka 814-0180, Japan*

(Received 18 February 2009; published 22 April 2009)

High-spin level structures of ^{94,95}Mo have been reinvestigated via the ^{16}O(^{82}Se, $xn\gamma$)^{94,95}Mo($x = 4, 3$) reactions at $E(^{82}\text{Se}) = 460$ MeV. The previously reported level schemes of these two nuclei have been largely modified up to ~11 MeV in excitation energy due to identifications of some important linking transitions. Shell-model calculations have been made in the model space of $\pi(p_{1/2}, g_{9/2}, d_{5/2})^4$ and $\nu(d_{5/2}, s_{1/2}, d_{3/2}, g_{7/2}, h_{11/2})^{2(3)}$ and compared with the modified level schemes. The structures of the newly assigned high-spin states in ^{94,95}Mo have been discussed.

DOI: 10.1103/PhysRevC.79.044316 PACS number(s): 21.10.Re, 23.20.Lv, 25.70.Gh, 27.60.+j

I. INTRODUCTION

The ^{94}Mo and ^{95}Mo nuclei ($Z = 42$, $N = 52, 53$) have a few valence particles outside the neutron ($N = 50$) and proton ($Z = 38$) subshell closure. These nuclei are expected to be spherical with similar level structures to those of neighboring nuclei that can be interpreted in terms of shell-model calculations. Actually, it has been shown that the low-lying levels of nuclei with $N = 50$ are dominated by the proton excitations within the $\pi(p_{1/2}, g_{9/2})$ or $\pi(f_{5/2}, p_{3/2}, p_{1/2}, g_{9/2})$ shell-model orbitals [1,2]. The medium-spin levels in $N > 50$ nuclei can be understood as the neutron excitations within the $\nu(d_{5/2}, s_{1/2}, d_{3/2}, g_{7/2}, h_{11/2})$ orbitals coupled to the valence proton configurations. Shell-model calculations [2–4] have shown that the neutron particle-hole excitation across the $N = 50$ shell gap must be taken into account to adequately describe the high-spin level structures of nuclei in the $N = 50$ region. As the neutron number increases, the level structure of molybdenum isotopes undergoes a change from spherical in ^{92}Mo to rotation-like in ^{104}Mo. Investigations of the high-spin level structures in ^{94,95}Mo would contribute to understanding the mechanisms responsible for the generation of high-spin states and probe the possible onset of collectivity in this mass region.

The high-spin states of ^{94,95}Mo were investigated a long time ago by Lederer *et al.* [5,6] and Mesko *et al.* [7] via $(\alpha, xn\gamma)$ reactions. The level schemes have been extended up to $I \sim 19$ at 12 MeV excitation energy by Kharraja and coworkers [4] using heavy-ion-induced fusion-evaporation reactions and the early implementation phase of the Gammasphere array. The results presented in the present article on ^{94,95}Mo were obtained as a by-product of the study of neutron-rich nuclei in ^{82}Se + ^{192}Os reactions. High-spin states of ^{94,95}Mo were populated via the ^{16}O(^{82}Se, $xn\gamma$)^{94,95}Mo($x = 4, 3$) reactions due to the oxidation of the thick ^{192}Os target. The previously reported level schemes [4] have been largely modified with the help of the high detection sensitivity of the GASP multidetector array [8]. During the course of this investigation, Chatterjee *et al.* reported a new level scheme of ^{95}Mo [9] in which the spin and parity assignments for some interesting energy levels were different from our result. In addition, we have carried out shell-model calculations up to high-spin states to understand the high-spin level structures of ^{94}Mo and ^{95}Mo. The Hamiltonian used in the shell-model calculations is determined so as to consistently reproduce overall energy levels of $40 \leqslant Z \leqslant 42$ and $50 \leqslant N \leqslant 53$ nuclei, including ^{94,95}Mo. The shell-model calculations explain well the energy levels newly assigned in this experiment; this allows us to discuss the structure of the high-spin states in ^{94,95}Mo.

II. EXPERIMENT

The experiment was devoted to investigate the high-spin states of neutron-rich nuclei through multinucleon transfer reactions in the ^{82}Se + ^{192}Os collision system at a bombarding energy of $E(^{82}\text{Se}) = 460$ MeV [10,11]. The beam was provided by the accelerator complex of the Tandem-XTU and the super conducting LINAC ALPI at the Laboratori Nazionali di Legnaro, Italy, and focused on an isotopically enriched ^{192}Os target of 60 mg/cm^2 thickness. Because the osmium foil was oxidized, high-spin states of ^{94,95}Mo were populated via the ^{16}O(^{82}Se, $xn\gamma$) ^{94,95}Mo($x = 4, 3$) reactions. The emitting γ rays from the reaction products were detected by the GASP multidetector array [8] that consists of 40 Compton suppressed large volume Ge detectors and a multiplicity filter of 80 BGO elements. The energy and efficiency calibrations were made using ^{59,60}Co, ^{133}Ba, and ^{152}Eu standard sources. Typical energy resolutions were about 2.0 ~ 2.5 keV at full

width at half maximum for the 1332.5-keV line. Events were collected when at least three suppressed Ge and two inner multiplicity filter detectors were fired. With these conditions a total of 1.5×10^9 events were recorded. After gain matching for all the detectors, the coincidence data were sorted into fully symmetrized matrices and cubes for subsequent off-line analysis.

The spins and parities of the levels were deduced, where possible, from angular distribution ratios as well as from the decay branches. To obtain multipolarity information for the emitted γ rays, two asymmetric coincidence matrices were constructed using the γ rays detected at all angles (y axis) against those observed at 34° (or 146°) and 90° (x axes), respectively. From these two matrices, the angular distribution asymmetry ratios, defined as $R_{\mathrm{ADO}}(\gamma) = I_\gamma(34^\circ)/I_\gamma(90^\circ)$, were extracted from the γ-ray intensities $I_\gamma(34^\circ)$ and $I_\gamma(90^\circ)$ in the coincidence spectra gated by the γ transitions (on the y axis) of any multipolarity. Usually, a single gate was used for strong peaks. For some weak or doublet peaks, the gating transitions were carefully chosen to obtain clear coincidence spectra in which possible contaminations to the transition of interest can be excluded. Stretched quadrupole transitions were adopted if $R_{\mathrm{ADO}}(\gamma)$ values were significantly larger than unity, and dipole transitions were assumed if $R_{\mathrm{ADO}}(\gamma)$'s were less than 1.0. It should be noted that uncertainties exist for the spin and parity assignments on the basis of the ADO ratio analysis; the stretched quadrupole transitions cannot be distinguished from $\Delta J = 0$ dipole transitions or certain mixed $\Delta J = 1$ transitions. In these cases, cross-checks from crossover or parallel transitions and their branching ratios provide supplementary arguments for the spin and parity assignments. In fact, a combination of the high statistics of three- and higher-fold coincidence events and the selective power of double-gating techniques makes it possible to identify and assign many crossover transitions in the proposed level scheme.

III. EXPERIMENTAL RESULTS

Most of the γ rays reported in the literature [4–7,9] have been observed in this experiment. The γ-ray coincidence relationships and their ADO ratios have been analyzed with care, leading to the establishment of the revised level schemes for ^{94}Mo that significantly differ from the previous work. This is mainly due to the identification of many new crossover or doublet transitions and their proper placements in the present level schemes with the help of double-gating techniques. Details of the modifications will be presented and explained in the following. The revised level schemes of ^{94,95}Mo and corresponding double-gated spectra are presented in Figs. 1–5. The measured spectroscopic data (γ-ray energies, relative intensities, ADO ratios, and suggested spin and parity assignments) are summarized in Table I and Table II.

A. Level scheme of ^{94}Mo

The present level scheme of ^{94}Mo is consistent with the previous result of Kharraja *et al.* [4] below the (12^+) and (13^-) levels. In addition, the newly observed γ rays of energy 504-, 671-, 1140-, 1168-, and 1307-keV have been assigned to connect the negative- and positive-parity levels. These new transitions can be clearly seen in Fig. 2. The 449-keV line de-exciting the second 6^+ state [5], which was not observed in Ref. [4], has been confirmed in this work. Based on the obtained ADO ratios, we have assigned an $E2$ multipolarity for the 1168- and 1307-keV γ rays, and an $E1$ transition for the 504- and 485-keV lines. These assignments lead to an identification of the second (8^+) and (10^+) levels at 3591-keV and 4262-keV excitation energies, respectively. The assignment of (10^+) to the 4262-keV level is further supported by the 366-keV, $\Delta J = 0$ dipole transition.

For the positive-parity levels above the (12^+) state, some important modifications have been made in the present level scheme as compared to the previous work of Kharraja *et al.* [4]. First the 1609-, 1060-, 973-, and 714-keV transitions were found to be quadrupole (see Table I) rather than dipole ones as suggested in Ref. [4]. Second, the ordering of γ rays in the intense 241-442-791-1244 transition sequence was changed in the present level scheme. This is supported by the observation of a new dipole (868-keV) and a new quadrupole (1658-keV) crossover transitions. Furthermore, the 1341- and 1740-keV transitions [4] have not been observed in this work. The 1367-keV line [4] should be the 1370-keV γ ray observed in this work. The energy and the placement of this line in the level scheme, i.e., $(19^+) \rightarrow (17^+)$, are supported by the new 928-keV, $(19^+) \rightarrow (18^+)$ transition.

A cascade of γ rays of energy 623-, 663-, 1062- and 2188-keV has been assigned to the present level scheme feeding the negative-parity levels. The ordering of these transitions is quite different from that proposed in Ref. [4] where the 663-keV γ ray was assigned as the $(14^-) \rightarrow (13^-)$ transition, and it was reported as having the same intensity as the 623- and 983-keV γ rays (see Table I of Ref. [4]). This cannot be confirmed in our work. One can see from the double-gated spectra of Fig. 2(a) that the 623-keV line is much stronger than the 663-keV γ ray. Therefore we have assigned the 623-keV transition to feed directly the (13^-) level and the latter on top of this cascade. In addition, the ADO values for the 623- and 663-keV γ rays are consistent with those of $\Delta J = 2$ quadrupole transitions, and it is reasonable to assign these two γ rays as the $(15^-) \rightarrow (13^-)$ and $(19^-) \rightarrow (17^-)$ transitions, respectively. The placement and ordering for the intense transitions are further supported by several crossover transitions as shown in Fig. 1.

Finally, it is worth noting that the γ-ray energies measured in our experiment were found to be different by up to 4 keV from the previous result [4]. For instance, the previously reported 2389-keV, $(13^+) \rightarrow (12^+)$ transition should be the 2384.6-keV γ ray observed in this work. Numerous γ rays emitted from the targetlike, projectile-like, and fusion-evaporation residues have been identified, and their energies determined in this work are consistent with the adopted values within an uncertainty of 0.5 keV. The larger uncertainties in γ-ray energies of Ref. [4] may be due to the thin target used in their experiment.

TABLE I. γ-ray transition energies, relative intensities, ADO ratios, and their assignments in ^{94}Mo.

E_γ(keV)[a]	I_γ[b]	R_{ADO}	$E_i \rightarrow E_f$ (keV)[c]	$J_i^\pi \rightarrow J_f^\pi$[d]
83.0			2955.2 → 2872.3	$8^+ \rightarrow 6^+$
240.8	152	0.70(6)	7788.7 → 7547.9	$(16^+) \rightarrow (15^+)$
251.0		1.68(22)	4747.2 → 4496.6	$(11^-) \rightarrow (11^+)$
293.4	700	1.69(10)	4190.4 → 3897.0	$12^+ \rightarrow 10^+$
306.3		0.76(10)	4496.6 → 4190.4	$(11^+) \rightarrow 12^+$
365.7	$\geqslant$280	1.73(10)	4262.4 → 3897.0	$(10^+) \rightarrow 10^+$
442.2	144	1.06(9)	9475.3 → 9033.1	$(18^+) \rightarrow (17^+)$
449.3	320	1.34(16)	2872.3 → 2423.0	$6^+ \rightarrow 6^+$
481.2	22		9033.1 → 8551.9	$(17^+) \rightarrow (16)$
484.8	405	0.92(6)	4747.2 → 4262.4	$(11^-) \rightarrow (10^+)$
503.7	76	0.89(16)	4094.8 → 3591.2	$(9^-) \rightarrow (8^+)$
532.2	1000	1.61(10)	2955.2 → 2423.0	$8^+ \rightarrow 6^+$
554.3	91	0.68(7)	6284.3 → 5730.0	$(14)^- \rightarrow (13^-)$
564.2	58		6848.5 → 6284.3	$(15^-) \rightarrow (14^-)$
567.0	18		7415.4 → 6848.5	$(16^-) \rightarrow (15^-)$
623.4	427	1.80(10)	6353.4 → 5730.0	$(15^-) \rightarrow (13^-)$
652.4	455	1.80(16)	4747.2 → 4094.8	$(11^-) \rightarrow (9^-)$
662.5	160	1.74(13)	10265.7 → 9603.2	$(19^-) \rightarrow (17^-)$
671.3	$\geqslant$42		4262.4 → 3591.2	$(10^+) \rightarrow (8^+)$
702.6	1900	1.74(12)	1573.5 → 870.9	$4^+ \rightarrow 2^+$
712.8	45		10265.7 → 9552.9	$(19^-) \rightarrow (18)$
714.4	97	1.58(14)	8607.5 → 7893.2	$(17^+) \rightarrow (15^+)$
728.2	423	1.77(15)	4094.8 → 3366.6	$(9^-) \rightarrow (7^-)$
756.5	261	1.80(13)	3366.6 → 2610.1	$(7^-) \rightarrow (5^-)$
766.0			11135.0 → 10369.0	
790.6	110	0.79(7)	10266 → 9475.3	$(19^+) \rightarrow (18^+)$
849.5	1626	1.64(11)	2423.0 → 1573.5	$6^+ \rightarrow 4^+$
867.7	135	0.90(10)	9475.3 → 8607.5	$(18^+) \rightarrow (17^+)$
870.9	$\geqslant$1900	1.74(10)	870.9 → 0	$2^+ \rightarrow 0^+$
928.0			10403.0 → 9475.3	$(19^+) \rightarrow (18^+)$
941.8	1105	1.73(9)	3897 → 2955.2	$10^+ \rightarrow 8^+)$
943.5	163	0.86(7)	3366.6 → 2423.0	$(7^-) \rightarrow 6^+$
973.1	127	1.67(14)	7547.9 → 6575	$(15^+) \rightarrow (13^+)$
982.8	612	1.68(13)	5730.0 → 4747.2	$(13^-) \rightarrow (11^-)$
1020.5			5210.9 → 4190.4	
1023.1			11135.0 → 10112.0	
1036.6	274	0.86(7)	2610.1 → 1573.5	$(5^-) \rightarrow 4^+$
1059.6	327	1.60(12)	8607.5 → 7547.9	$(17^+) \rightarrow (15^+)$
1062.0	220	0.72(6)	7415.4 → 6353.4	$(16^-) \rightarrow (15^-)$
1139.6	120	0.77(8)	4094.8 → 2955.2	$(9^-) \rightarrow 8^+$
1168.2	151	1.43(11)	3951.2 → 2423.0	$(8^+) \rightarrow 6^+$
1244.4	132	1.10(10)	9033.1 → 7788.7	$(17^+) \rightarrow (16^+)$
1307.2	$\geqslant$87	1.67(20)	4262.4 → 2955.2	$(10^+) \rightarrow 8^+$
1364.3			6575.0 → 5210.9	
1370.0			10403.0 → 9475.3	
1428.8	132	1.60(10)	7782.2 → 6353.4	$(17^-) \rightarrow (15^-)$
1504.2			10112.0 → 8607.5	
1540.0	60	0.76(9))	5730.0 → 4190.4	$(13^-) \rightarrow 12^+$
1608.0			8456.5 → 6848.5	
1609.4	577	1.65(11)	5799.8 → 4190.4	$(14^+) \rightarrow 12^+$
1658.4	50	1.49(20)	10265.7 → 8607.5	$(19^+) \rightarrow (17^+)$
1692	11		9475.3 → 7782.2	$(18^+) \rightarrow (17^-)$
1748.1	362	1.48(12)	7547.9 → 5799.8	$(15^+) \rightarrow (14^+)$
1761.4			10369.0 → 8607.5	
1770.7	31		9552.9 → 7782.2	$(18) \rightarrow (17^-)$
1820.5	14		9603.2 → 7782.2	$(17^-) \rightarrow (17^-)$
1912.0			10369 → 8456.5	

TABLE I. *(Continue.)*

E_γ(keV)[a]	I_γ[b]	R_{ADO}	$E_i \rightarrow E_f$ (keV)[c]	$J_i^\pi \rightarrow J_f^\pi$[d]
2093.4	97	1.26(11)	7893.2 → 5799.8	$(15^+) \rightarrow (14^+)$
2137.5			9552.9 → 7414.4	$(18) \rightarrow (16^-)$
2187.8	143	1.40(12)	9603.2 → 7415.4	$(17^-) \rightarrow (16^-)$
2198.5	17		8551.9 → 6353.4	$(17^+) \rightarrow (15^-)$
2384.6	97	1.47(12)	6575 → 4190.4	$(13^+) \rightarrow 12^+$

[a]Uncertainties are within 0.5 keV.
[b]Uncertainties are within 30%.
[c]Excitation energies of initial E_i and final E_f states.
[d]Proposed spin and parity assignments for the initial J_i^π and final J_f^π levels.

TABLE II. γ-ray transition energies, relative intensities, ADO ratios, and their assignments in ^{95}Mo.

E_γ(keV)[a]	I_γ[b]	R_{ADO}	$E_i \rightarrow E_f$ (keV)[c]	$J_i^\pi \rightarrow J_f^\pi$[d]
38.0			2618.7 → 2580.4	$(19/2^+) \rightarrow (17/2^+)$
151.7	770	0.86(21)	2770.4 → 2618.7	$(21/2^+) \rightarrow (19/2^+)$
174.0	⩾30		2232.4 → 2058.5	$(15/2^+) \rightarrow (13/2^+)$
348.0	800	0.86(5)	2580.4 → 2232.4	$(17/2^+) \rightarrow (15/2^+)$
386.0	⩾80	0.8512	1937.7 → 1551.7	$11/2^- \rightarrow (9/2^+)$
386.3	67	1.6324	2618.7 → 2232.4	$(19/2^+) \rightarrow (15/2^+)$
467.5	300	1.65(18)	4140.2 → 3672.9	$(29/2^+ \rightarrow (25/2^+)$
522.0	60		2580.4 → 2058.5	$(17/2^+) \rightarrow (13/2^+)$
534.5	85	0.5410	7985.1 → 7451.4	$(39/2^-) \rightarrow (37/2^-)$
553.0	⩾40		2611.5 → 2058.5	$(15/2^-) \rightarrow (13/2^+)$
593.2	550	0.80(11)	1540.9 → 947.7	$11/2^+ \rightarrow 9/2^+$
604.0	⩾50		1551.7 → 947.7	$(9/2^+) \rightarrow 9/2^+$
643.0	390	1.92(16)	5760.4 → 5117.4	$(31/2^-) \rightarrow (27/2^-)$
666.0	⩾147	1.80(20)	3277.5 → 2611.5	$(19/2^-) \rightarrow (15/2^-)$
673.8	⩾72	2.07(25)	2611.5 → 1937.7	$(15/2^-) \rightarrow 11/2^-$
691.5	1000	1.65(14)	2232.4 → 1540.9	$(15/2^+) \rightarrow 11/2^+$
742.6	110	1.12(13)	7451.4 → 6708.6	$(37/2^-) \rightarrow (35/2^-)$
765.8	⩾450	0.90(8)	765.8 → 0	$7/2^+ \rightarrow 5/2^+$
770.6	⩾128	1.90(35)	4048.1 → 3277.5	$(23/2^-) \rightarrow (19/2^-)$
774.4	450	1.60(13)	1540.9 → 765.8	$11/2^+ \rightarrow 7/2^+$
785.9			1551.7 → 765.8	$(9/2^+) \rightarrow (7/2^+)$
854.2	120	1.45(15)	10508.6 → 9654.4	$(45/2^-) \rightarrow (43/2^-)$
902.5	730	1.70(14)	3672.9 → 2770.4	$(25/2^+) \rightarrow (21/2^+)$
947.7	⩾1220	2.20(40)	947.7 → 0	$9/2^+ \rightarrow 5/2^+$
948.2	390	1.56(37)	6708.6 → 5760.4	$(35/2^-) \rightarrow (31/2^-)$
965.7	125	1.74(29)	6327.8 → 5362.1	$(35/2^+) \rightarrow (31/2^+)$
1069.5	125	1.60(15)	5117.4 → 4048.1	$(27/2^-) \rightarrow (23/2^-)$
1110.8	⩾90	1.70(28)	2058.5 → 947.7	$(13/2^+) \rightarrow 9/2^+$
1221.9	258	0.65(10)	5362.1 → 4140.2	$(31/2^+) \rightarrow (29/2^+)$
1276.5	125	1.78(20)	7985.1 → 6708.6	$(39/2^-) \rightarrow (35/2^-)$
1445.1	227	0.85(8)	5117.4 → 3672.9	$(27/2^-) \rightarrow (25/2^+)$
1669.3	160	1.15(18)	9654.4 → 7985.1	$(41/2^-) \rightarrow (39/2^-)$
2097.0	65	1.36(28)	8424.8 → 6327.8	$(37/2^+) \rightarrow (35/2^+)$

[a]Uncertainties are within 0.5 keV.
[b]Uncertainties are within 30%.
[c]Excitation energies of initial E_i and final E_f states.
[d]Proposed spin and parity assignments for the initial J_i^π and final J_f^π levels.

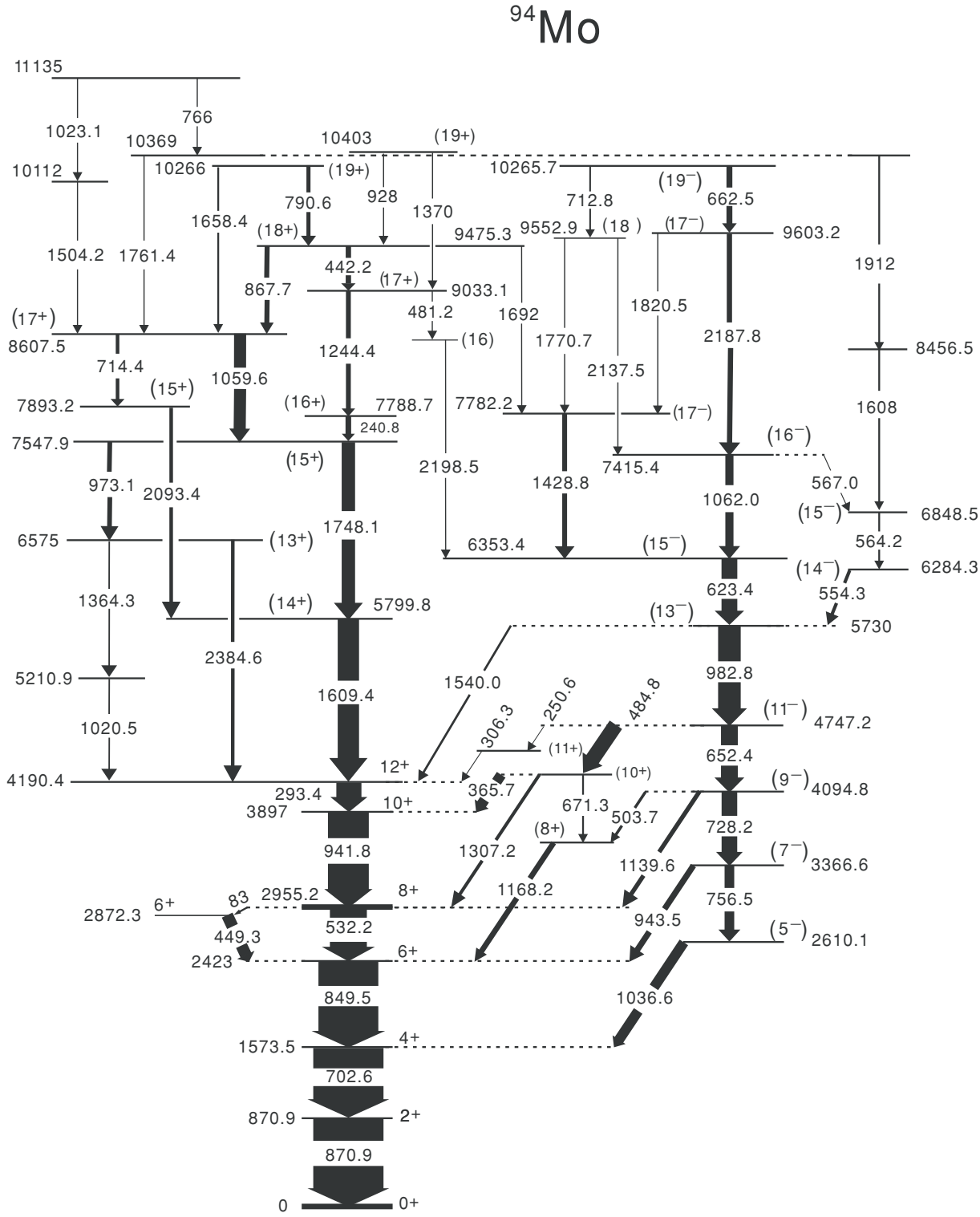

FIG. 1. Level scheme of ^{94}Mo deduced from this work.

B. Level scheme of ^{95}Mo

Up to the $(17/2^+)$ level at 2580 keV and the $(15/2^-)$ level at 2612 keV, our results are consistent with the earlier work of Refs. [6,7]. However, the strong dipole transition of 152 keV had been placed to feed directly the $(17/2^+)$ level at 2580 keV [4,6,7]; this is not consistent with our work considering the γ-γ coincidence relationships. From the double-gated spectra shown in the upper and middle panels of Fig. 4, the existence of a 386-keV transition can be confirmed and assigned as parallel to the 348-keV, $(17/2^+) \rightarrow (15/2^+)$

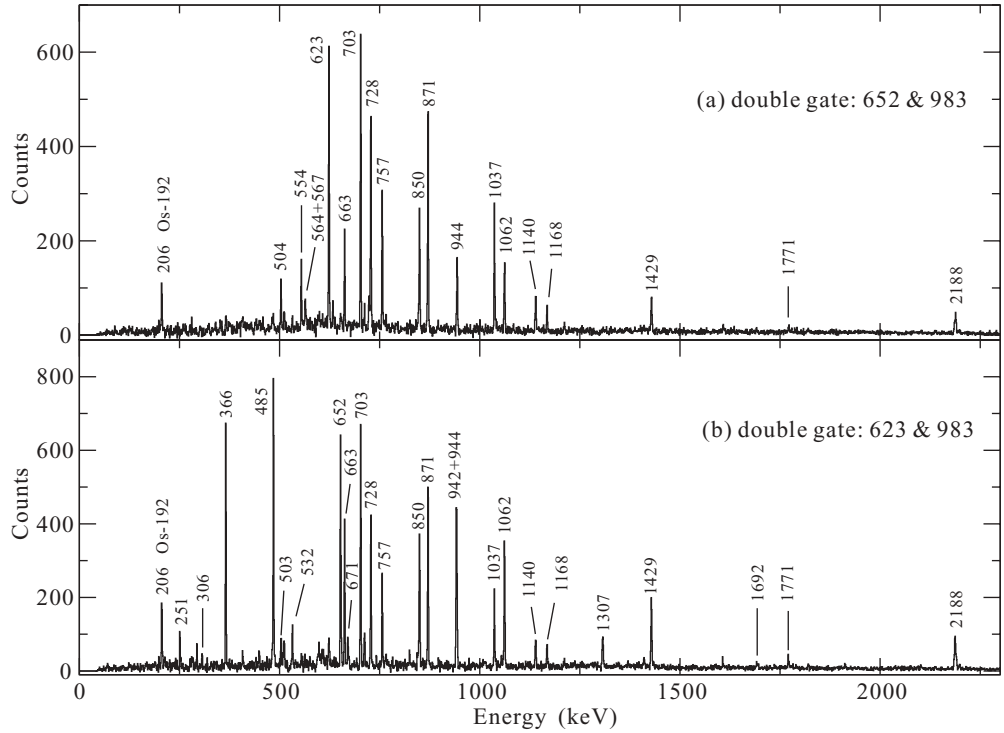

FIG. 2. Double-gated coincidence spectra for ^{94}Mo.

transition. In fact, the 386-keV line was reported as a doublet [6], and the authors of Refs. [6,7] had assigned one of them in the low-lying level scheme corresponding to the $11/2^- \rightarrow (9/2^+)$ transition, leaving one 386-keV γ ray unassigned. The ADO ratio analysis shows that the second 386-keV transition has a quadrupole multipolarity (see Table II), and we have therefore assigned this 386-keV γ ray as a $(19/2^+) \rightarrow (15/2^+)$ transition. Subsequently, the 152- and 903-keV γ rays have been assigned as $(21/2^+) \rightarrow (19/2^+)$ and $(25/2^+) \rightarrow (21/2^+)$ transitions, respectively. The $(19/2^+) \rightarrow (17/2^+)$ transition may be highly converted and the low-energy γ ray of 38 keV could be out of the detection limit of GASP. It is noted that the *yrast* levels become $(19/2^+)$, $(21/2^+)$, and $(25/2^+)$ if our spin assignments are adopted for the 2619-, 2770-, and 3673-keV levels. This is in perfect agreement with the shell-model predictions (see Refs. [4,6] and Sec. IV C in this article). Above the $(25/2^+)$ state, the 468-, 1222-, 966-, and 2097-keV γ rays have been assigned to de-excite the positive-parity levels according to their ADO ratios and relative intensities. The 1445-keV γ ray is considered to be a linking transition between negative- and positive- parity states; this is explained in the following paragraph.

The $11/2^-$ and $(15/2^-)$ assignments have been proposed in Refs. [6,7] for the levels at 1938- and 2612-keV excitation energies. It is worth noting that the $11/2^-$ assignment was supported by the ^{94}Mo$(d, p)^{95}$Mo transfer reaction data that indicate an appreciable fraction of $h_{11/2}$ single-particle strength for a level at 1930 keV [12]. The linking transitions (174-, 522-, 553-, and 1111-keV lines) [6,7] connecting the low-lying positive- and negative-parity levels have been confirmed in our double-gated coincidence spectra. Accepting the $11/2^-$ and $(15/2^-)$ assignments for the 1938- and 2612-keV levels [6,7,12], the negative-parity states have been extended up to $(27/2^-)$ at 5117 keV taking into account of the quadrupole character of 666-, 771-, and 1070-keV transitions.

Above the $(27/2^-)$ state, a strong transition sequence consisting of 643-, 948-, 1277-, 1669-, and 854-keV γ rays was observed. The ADO ratio analysis shows that they are quadrupole transitions and thus have been assigned as de-exciting the negative-parity levels as shown in the level scheme. The γ-ray flux is fragmented from the $(27/2^-)$ state to both the positive- and negative-parity levels through the 1445- and 1070-keV transitions, respectively. The ADO ratio for the 1445-keV γ ray has been checked with care, and it is found to be a dipole transition in agreement with Ref. [9]. This γ ray is assigned as an $E1$, $(27/2^-) \rightarrow (25/2^+)$ transition, which provides in turn a supplementary argument for the observation of the 386-keV, $(19/2^+) \rightarrow (15/2^+)$ transition.

One may notice that the present level scheme differs largely from that of Ref. [4] at high spins not only in the level ordering, spin and parity assignments but some important coincidence relationships as well. For instance, the γ transition sequences (1) and (2) of Ref. [4] were proposed to de-excite the positive-parity levels, and the two sequences were connected at the $(27/2^+)$ state that de-excites via 535- and 387-keV γ transitions. From the coincidence spectra shown in Fig. 4 and 5, it seems unreasonable to place the 535- and 950-keV (it should be 948.2-keV rather than the ground-state transition of 947.7 keV) transitions to the same locations of previous level scheme [4]. We found that the relative intensities of 535- and 948.2-keV γ rays are much weaker than the reported values in Ref. [4]. This is evident in the lower panel of Fig. 4 that

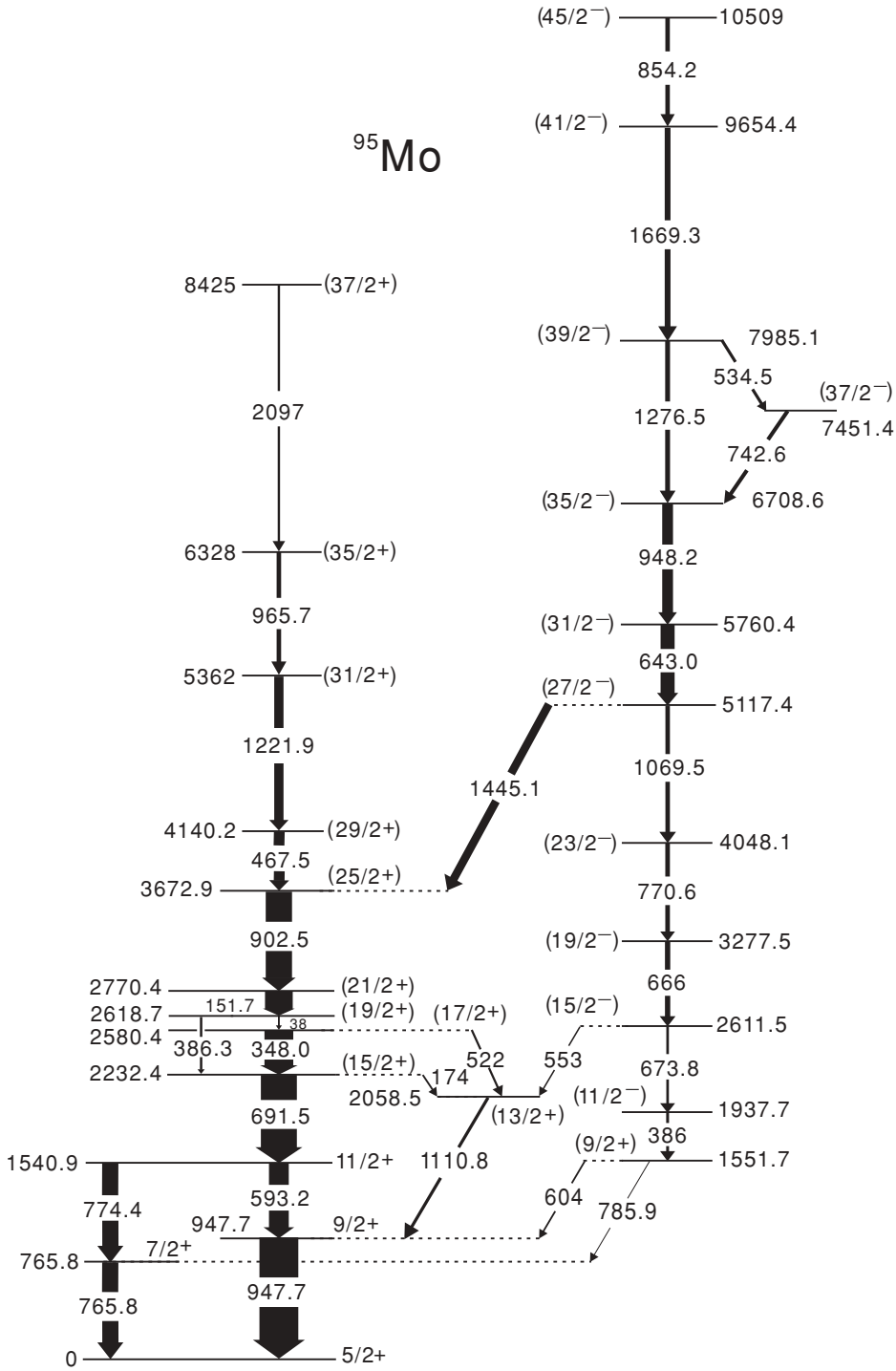

FIG. 3. Level scheme of ^{95}Mo deduced from this work.

the intensity of the high-lying 535-keV/(948-keV) transition is less than 10%/(50%) rather than 70%/(108%) [4] of the intensity of the 903-keV transition. To check the intensity balance of the 535-keV transition, we present the 643- and 948-keV double-gated spectrum in Fig. 5(a), where one can see that the 535-keV line is too weak to be placed in the main decay path as proposed in Ref. [4]. Furthermore, self-coincidence of the 535-keV transition could not be confirmed in our data, leading to the conclusion that the proposed 535-keV, $(27/2^+) \rightarrow (25/2^+)$ transition in Ref. [4] does not exist. This makes it questionable for the connection point at the $(27/2^+)$ level for the two parallel transition sequences [4]. In addition, the 468-1222-966 cascade is connected directly with the 903-keV transition rather than with the higher-lying 948.2-keV

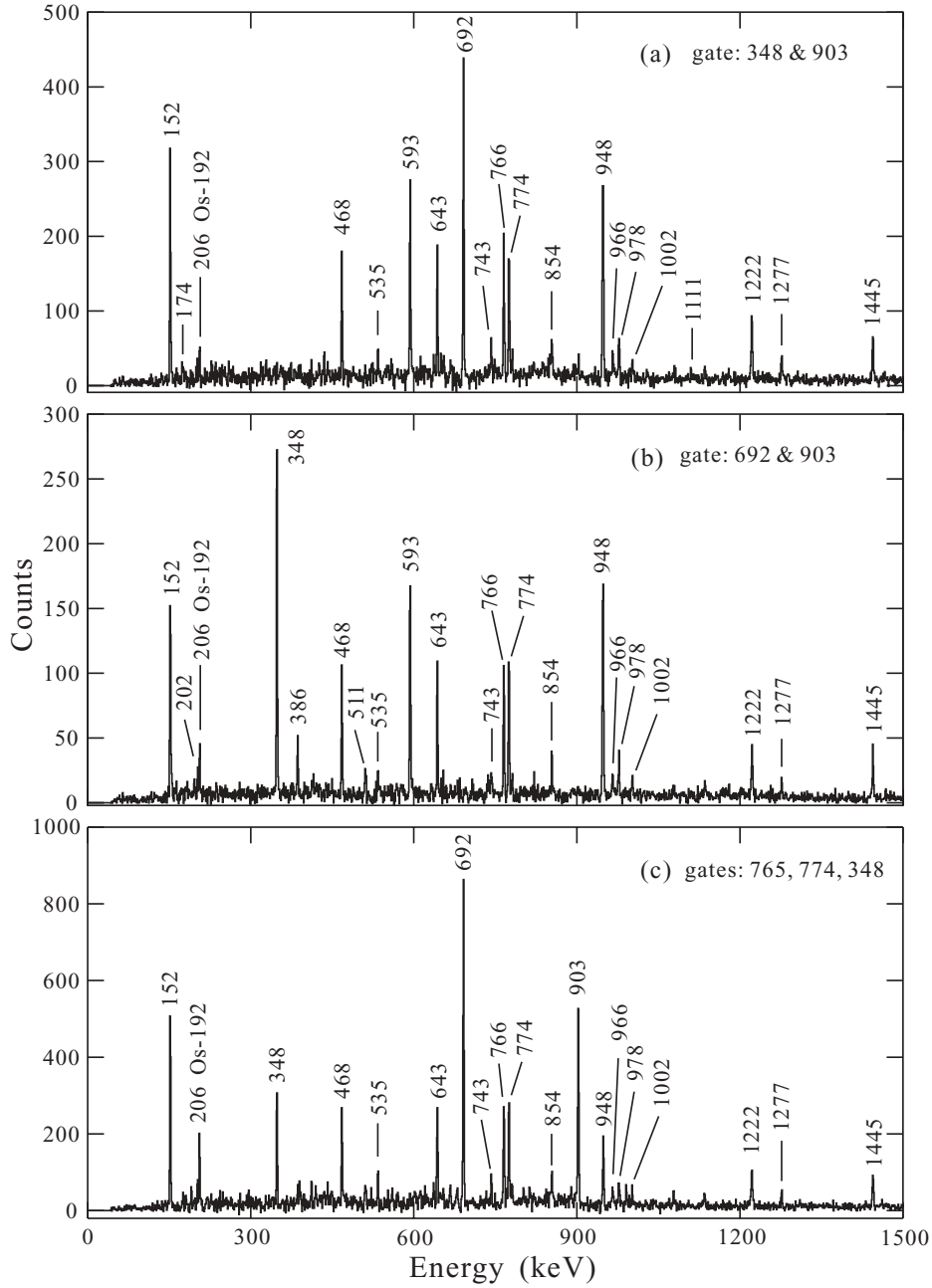

FIG. 4. Typical double-gated coincidence spectra for ^{95}Mo.

transition. This can be concluded simply by comparing the relative intensities of the 948- and 903-keV lines in Fig. 5(b) with that in Fig. 5(c).

A sequence of negative-parity levels in ^{95}Mo was reported in Ref. [4] being constructed by the 760-, 1037-, 1266-, 1500-, and 1531-keV γ transitions of $E2$ character. These γ rays have been observed also in this experiment. However, they were found to be much stronger than the yrast transitions in ^{95}Mo. In our data set, the energy resolution was better than the thin-target experiment [4]. The above-mentioned γ rays were found to be in coincidence with the 385.5- and 949.7-keV γ lines rather than the 386- and 948-keV transitions in ^{95}Mo. We have assigned this cascade to ^{93}Nb that was produced via the ^{16}O(^{82}Se, $p4n$)^{93}Nb reaction in our experiment. It is not impossible that this nucleus might be produced in Ref. [4] through the ^{65}Cu(^{36}S,2α)^{93}Nb reaction.

The proposed level scheme of ^{95}Mo is not fully consistent with the recent work of Chatterjee *et al.* [9]. The main discrepancies concern the spin and parity assignments for some important energy levels. First, the weak 386-keV transition is found to be quadrupole rather than dipole [9], leading to the assignment of $(19/2^+)$ for the level at 2619 keV. As mentioned in the previous paragraph, the level spacing and ordering for the $(19/2^+)$, $(21/2^+)$, and $(25/2^+)$ *yrast* states can be well reproduced by the shell-model calculations (see Refs. [4,6] and Sec. IV C in this article). Second, the 674-,

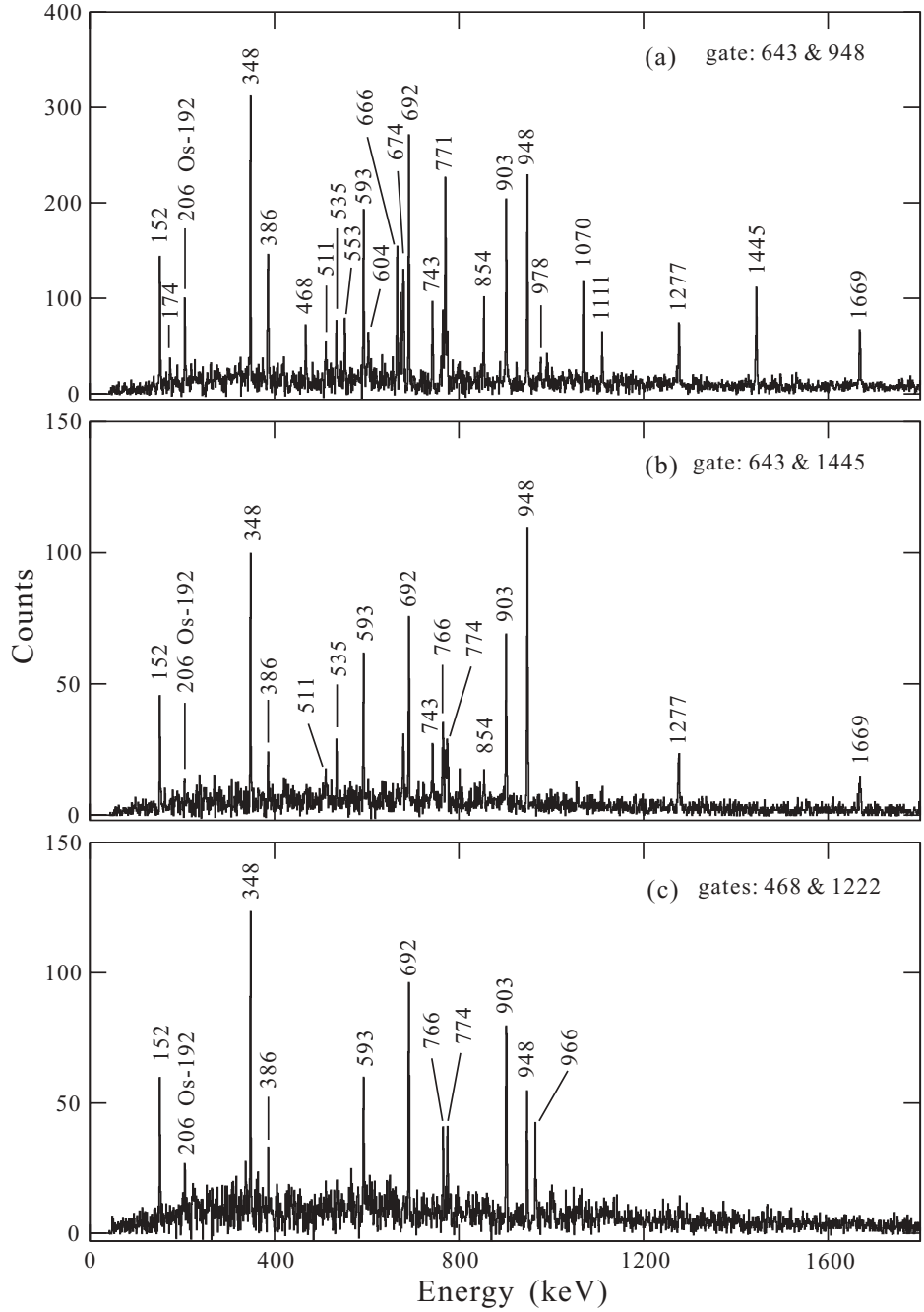

FIG. 5. Typical double-gated coincidence spectra for ^{95}Mo.

666-, 771-, and 1070-keV transitions have been determined to be quadrupole in this experiment, which is consistent with Ref. [4], while $\Delta J = 1$ assignments were proposed [9] for the 674- and 771-keV transitions. The $\Delta J = 2$ assignment for the 674-keV transition was also adopted in Refs. [6,7]. We accept the previously proposed $11/2^-$ and $(15/2^-)$ assignments [6,7,12] for the 1938- and 2612-keV levels, leading to $(27/2^-)$ rather than $25/2^+$ [9] for the 5117-keV level. The observation of the 1445-keV, $(27/2^-) \rightarrow (25/2^+)$ linking transition provides an argument for the present spin and parity assignments. We note that a sequence of negative-parity levels based on the $11/2^-$ state has been found in ^{97}Mo [9,13].

IV. SHELL-MODEL CALCULATIONS AND DISCUSSIONS

A. Shell-model calculations

The shell model seems to be an appropriate tool to study the structure of ^{94,95}Mo. However, there is not any effective interaction reliable for analyzing the high-spin states under consideration. We therefore employ the shell model with extended $P + QQ$ interaction [14,15]. The readers are referred to Refs. [14,15] for details.

We take three proton single-particle states ($p_{1/2}$, $g_{9/2}$, $d_{5/2}$) and five neutron single-particle states ($d_{5/2}$, $s_{1/2}$, $d_{3/2}$, $g_{7/2}$, $h_{11/2}$) as a model space. By studying the single-particle

energies used in Refs. [16–19], we fixed their energies in MeV as follows: $\varepsilon_{p1/2} = 0.0$, $\varepsilon_{g9/2} = 1.9$, $\varepsilon_{d5/2} = 4.2$, for protons; $\varepsilon_{d5/2} = 0.0$, $\varepsilon_{s1/2} = 1.86$, $\varepsilon_{d3/2} = 2.43$, $\varepsilon_{g7/2} = 2.50$, $\varepsilon_{h11/2} = 3.70$ for neutrons. The energy difference $\varepsilon_{g9/2} - \varepsilon_{p1/2} = 0.9$ for protons used in Refs. [16–19] is modified to be 1.9 MeV to reproduce correctly the $9/2^+$ and $1/2^-$ states in ^{91,93}Nb. (We note that the strong $J = 0$ pairing interaction in the $g_{9/2}$ orbital as compared with the small one in the $p_{1/2}$ orbital significantly affects the relative positions of the $9/2^+$ and $1/2^-$ states in odd-proton nuclei). We include the $d_{5/2}$ orbital in the proton space, because this orbital is considered to join considerably in correlations when nucleons occupy the $g_{9/2}$ orbital [20,21]. The neutron single-particle energies are also changed a little so as to roughly reproduce the change in level scheme as the neutron number increases in calculations for heavier nuclei with $N > 53$.

The strengths of the $J = 0$ and $J = 2$ pairing forces, QQ force, and octupole-octupole force are determined so that the same set of parameters reproduces the observed energy levels as a whole in lighter isotopes of Zr, Nb, and Mo including odd-A and odd-odd nuclei ($40 \leqslant Z \leqslant 42$, $50 \leqslant N \leqslant 53$). We use different force strengths for proton-proton (pp) interactions and for neutron-neutron (nn) and neutron-proton (np) interactions and impose A dependence on them as usual. Note that the present treatment does not conserve the isospin in contrast to the previous extended $P + QQ$ model calculations for $N \approx Z$ nuclei using isospin-invariant Hamiltonian [14,15,20,21]. We adopt an approximation that the nn and np interactions have the same force strengths g_0, g_2, χ_2, and χ_3 to reduce the number of parameters. The fixed parameters are as follows (in MeV): $g_0 = 25/A$, $g_2 = 260/A^{5/3}$, $\chi_2 = 300/A^{5/3}$, $\chi_3 = 200/A^6$ for pp interactions; $g_0 = 20/A$, $g_2 = 260/A^{5/3}$, $\chi_2 = 200/A^{5/3}$, $\chi_3 = 200/A^6$ for nn and np interactions. To improve the level schemes in ^{91}Nb and ^{92}Mo, we add two monopole corrections to the proton interactions, $\Delta k^{T=1}(p^\pi_{1/2}, p^\pi_{1/2}) = -0.45$ and $\Delta k^{T=1}(g^\pi_{9/2}, g^\pi_{9/2}) = -0.25$ in MeV. The first one strengthens the pairing interaction in the $p_{1/2}$ orbital on behalf of the pairing correlations in the fp shell. If this correction is not adopted, the $1/2^-$ level becomes lower than the $9/2^+$ level in ^{91}Nb even though the energy difference $\varepsilon_{g9/2} - \varepsilon_{p1/2}$ is taken to be large as 1.9 MeV. The monopole correction $\Delta k^{T=1}(g^\pi_{9/2}, g^\pi_{9/2})$ improves the two-body interaction matrix elements for the $g_{9/2}$ orbital and lowers better the second exited state of each J in ^{92}Mo.

We use the shell-model code NuShellX newly released by W. Rae [22]. This code first obtains proton and neutron substates and then diagonalizes np interactions for their product states. The code NuShellX is suitable for our study of Mo isotopes in which valence protons and neutrons occupy different shells.

Calculated results for 12 nuclei are satisfactory although we show only the results for ^{94}Mo and ^{95}Mo in this article. Details of the present calculations in ^{94,95}Mo and neighboring nuclei will be reported in a separate article. We note here that changes of force strengths within 10% do not significantly affect the level schemes of ^{94}Mo and ^{95}Mo. The present model is suitable for discussing the structure of ^{94,95}Mo.

B. Structure of ^{94}Mo

Calculated energy levels for ^{94}Mo are compared with experimental ones in Fig. 6 for positive- and negative-parity states, where the two lowest-energy levels of each spin J ($J^+_{1,2}$, $J^-_{1,2}$) are shown. Some of the experimental data are taken from the evaluated nuclear structure data file (ENSDF) [23]. The agreement between calculation and experiment is satisfactory for both the positive- and negative-parity states.

The calculation reproduces well not only the yrast band ($0^+_1, 2^+_1, \ldots 12^+_1$) but also the second band ($0^+_2, 2^+_2, \ldots 10^+_2$) at low energy except that the 8^+_1 state lies lower than the 6^+_1 state in the calculated result. The inverse order of the 6^+_1 and 8^+_1 levels is due to the defect that the QQ force does not give a good value for the interaction matrix element $\langle (g_{9/2})^2_{J=8} | V | (g_{9/2})^2_{J=8} \rangle$ as stated in Ref. [14]. If we set $\langle (g_{9/2})^2_{J=8} | V | (g_{9/2})^2_{J=8} \rangle$ to be a slightly repulsive value, we can get the correct order of the 6^+_1 and 8^+_1 levels. However, we have not implemented this manipulation.

The experimental values of $B(E2; 2^+_1 \to 0^+_1)$ and $B(E2; 4^+_1 \to 2^+_1)$ are 16.0(4) and 26(4) in W.u. [23]. These values indicate that these states are considerably collective for the $4p$-$2n$ system. In Fig. 6, relative values of calculated $B(E2)$ are shown using the widths of arrows. We used the effective charge $e_p = 2.1e$ for protons and $e_n = 1.0e$ for neutrons so as to reproduce the observed $B(E2; 2^+_1 \to 0^+_1) \approx 16$. The calculated value of $B(E2; 4^+_1 \to 2^+_1)$ is smaller than the observed one and the abrupt decrease of $B(E2; 6^+_1 \to 4^+_1)$ in the calculation is in disagreement with experiment, which suggests insufficiency of our model space.

Let us discuss the structure of the yrast states. Table III shows the leading component of configurations $(p^4)^\pi_{Jp}(n^2)^\pi_{Jn}$ (π being the parity of proton and neutron subsystems), its squared amplitudes, and expectation values of proton numbers $\langle n_a \rangle_p$ and neutron numbers $\langle n_a \rangle_n$ in the respective orbitals a. To understand the structure of ^{94}Mo in connection with Table III, we show the eigenstates of proton and neutron subsystems corresponding to ^{92}Mo and ^{90}Sr, in Fig. 7 in which the energy levels of the $4p$ system (^{92}Mo) and the $2n$ system (^{90}Sr) are basically well reproduced by our Hamiltonian. The calculation does not reproduce some energy levels observed in ^{90}Sr. These states, however, seem to be excited states of protons from the lower fp orbitals neglected in our model space. In our treatment, the eigenstates of ^{94}Mo are combinations of the product states of proton and neutron states shown in Fig. 7.

We can see in Table III that the structure of the yrast band changes slightly at the 6^+_1 state. This is because two neutrons can have the maximum spin $J = 4$ at low energy (see Fig. 7), because the Fermi level lies at the $d_{5/2}$ orbital and the excitation of a neutron into the $g_{7/2}$ orbital needs more energy. This causes the decrease of $B(E2; 6^+_1 \to 4^+_1)$ mentioned above. From Table III, we understand that proton and neutron distributions over the single-particle orbitals are similar to each other up to $J \leqslant 12$. The differences come from the angular-momentum coupling.

The present experiment obtained a level scheme that is significantly different from previous one [4]. The newly assigned high-spin states, therefore, should be the focus of our study. The level at 5.8 MeV is a key state when we construct

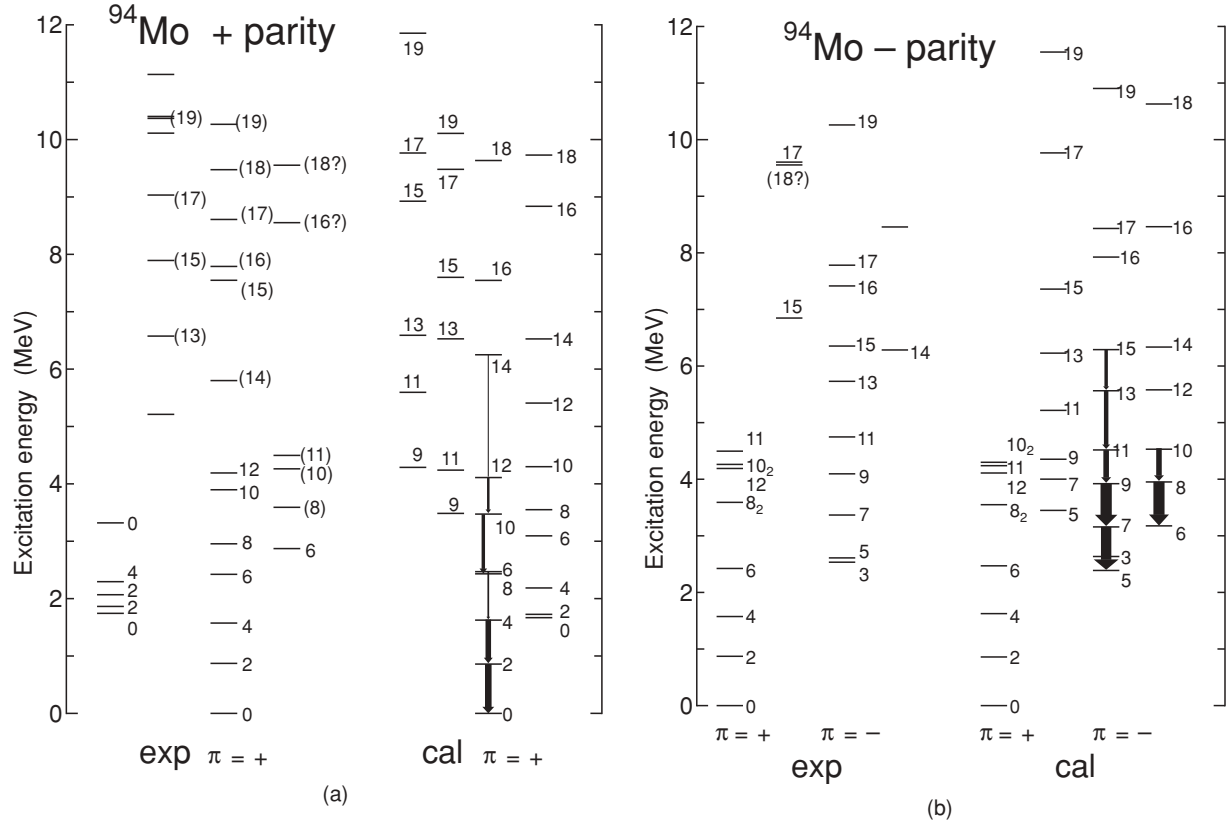

FIG. 6. Calculated positive- and negative-parity energy levels of ^{94}Mo, which are compared with experimental ones. The widths of the arrows denote relative values of $B(E2)$.

the level scheme above the 12^+_1 state. This state was assigned as a 13^+ state in Ref. [4]. However, in our search for good parameter sets for Zr, Nb, and Mo isotopes with $N \leqslant 53$, the 14^+_1 state always lies below the 13^+_1 state in ^{94}Mo when we change the force strengths. Therefore, the state at 5.8 MeV is probably the 14^+_1 state as the present experiment assigns.

Because the calculated results basically correspond to the experimental observations, let us discuss the structure of the observed high-spin states. Table III indicates that high-spin states get large angular momentum from the proton configurations, because the two neutrons cannot give spin $J > 4$ at low energy. The four protons can supply spin $J = 12$ at most but the energy becomes large when $J > 8$. In Table III, therefore, the 13^+_1 and 14^+_1 states are constructed by changing the $2n$ configurations, i.e., by one neutron jumping into the $g_{7/2}$ orbital. Next, the 15^+_1 and 16^+_1 states are constructed by changing the $4p$ configurations, i.e., by four protons occupying the $g_{9/2}$ orbital, because the two neutrons in the $d_{5/2}$ and $g_{7/2}$ orbitals cannot have spin $J > 6$. For the higher-spin states $17^+_1, 18^+_1$, and 19^+_1, it is an efficient way to have the $2n$ configuration of $(d_{5/2}h_{11/2})^{\pi=-}$ with high spin.

The calculated $17^+_1, 18^+_1$, and 19^+_1 states are at reasonably good energies. This means that the energy spacing $\varepsilon_{h11/2} - \varepsilon_{d5/2}$ should not be decreased with respect to the present value. Similarly, the calculated 13^+_1 and 14^+_1 states are roughly at the experimental energies. It does not seem appropriate to further decrease the energy spacing $\varepsilon_{g7/2} - \varepsilon_{d5/2}$. This is probable if we consider possible contributions from the neutron $g_{9/2}$ orbital that is excluded in our truncated space. We can therefore say that it is appropriate to have the $g_{7/2}$ orbital above the $s_{1/2}$ orbital and nearby the $d_{3/2}$ orbital as in Refs. [16–19]. In fact, we lowered the $g_{7/2}$ orbital near to the $d_{3/2}$ orbital to get the 14^+_1 state at better position. This makes the 13^+_1 and 14^+_1 states have the wave functions tabulated in Table III. If we take the energy spacing $\varepsilon_{g7/2} - \varepsilon_{d3/2} = 0.4$ MeV as in Refs. [16–19], the leading configuration of the 13^+_1 and 14^+_1 states is $(p^4)^+_{10}(n^2)^+_4$, which has four protons in the $g_{9/2}$ orbital like the 15^+_1 and 16^+_1 states.

We have calculated $B(E2)$ values also for high-spin states. Unfortunately, these $B(E2)$ values between the high-spin states are much smaller than those between the yrast states with $J \leqslant 12$. For instance, $B(E2; 14^+_1 \rightarrow 12^+_1)$ is 0.54 W.u. and most of other $B(E2; J^+_1 \rightarrow J'^+_1)$ values are very small. We cannot make a meaningful comparison between the calculated $B(E2)$ values and observed transition strengths. The degrees of freedom are probably too small for high-spin states in our truncated space. The calculation gives large $B(M1)$ values (more than 3 μ^2_N) for the transitions $11^+_1 \rightarrow 12^+_1$, $16^+_1 \rightarrow 15^+_1$, and $18^+_1 \rightarrow 17^+_2$. This is consistent with the experimental observation of these transitions in spite of the relatively narrow energy spacings.

On further consideration, although our shell model reproduces the basic level scheme even for the high-spin states, neutron excitations from the $g_{9/2}$ orbital must contribute

TABLE III. Structure of the yrast states with positive parity in ^{94}Mo. The leading component of configurations $(p^4)^{\pi}_{Jp}(n^2)^{\pi}_{Jn}$ and its squared amplitude (in percentages) are tabulated in the third and second columns, where the superscript π in $(p^4)^{\pi}_{Jp}(n^2)^{\pi}_{Jn}$ means the parity of the $4p$ and $2n$ subsystems. Expectation values of proton number $\langle n_a\rangle$ (neutron number $\langle n_a\rangle$) in three proton orbitals (in five neutron orbitals) are tabulated in columns 4–6 (in columns 7–11).

J^{π}_i	Leading config.		Proton $\langle n_a\rangle_p$			Neutron $\langle n_a\rangle_n$				
	%	$(p^4)^{\pi}_{Jp}(n^2)^{\pi}_{Jn}$	$p_{1/2}$	$g_{9/2}$	$d_{5/2}$	$d_{5/2}$	$s_{1/2}$	$d_{3/2}$	$g_{7/2}$	$h_{11/2}$
0^+_1	86	$(p^4)^+_0(n^2)^+_0$	1.60	2.27	0.13	1.72	0.13	0.07	0.07	0.01
2^+_1	71	$(p^4)^+_0(n^2)^+_2$	1.62	2.26	0.13	1.75	0.15	0.06	0.04	0.01
4^+_1	78	$(p^4)^+_0(n^2)^+_4$	1.64	2.24	0.12	1.91	0.05	0.02	0.01	0.01
6^+_1	71	$(p^4)^+_6(n^2)^+_0$	1.82	2.10	0.07	1.71	0.15	0.07	0.06	0.01
8^+_1	80	$(p^4)^+_8(n^2)^+_0$	1.82	2.15	0.03	1.73	0.13	0.07	0.06	0.01
10^+_1	88	$(p^4)^+_8(n^2)^+_2$	1.78	2.19	0.03	1.74	0.17	0.05	0.03	0.01
12^+_1	99	$(p^4)^+_8(n^2)^+_4$	1.83	2.16	0.01	1.97	0.00	0.02	0.00	0.01
11^+_1	97	$(p^4)^+_8(n^2)^+_4$	1.81	2.18	0.01	1.96	0.02	0.00	0.00	0.01
13^+_1	77	$(p^4)^+_8(n^2)^+_6$	1.42	2.56	0.02	1.17	0.01	0.01	0.81	0.00
14^+_1	98	$(p^4)^+_8(n^2)^+_6$	1.83	2.16	0.01	1.00	0.00	0.00	0.99	0.00
15^+_1	98	$(p^4)^+_{12}(n^2)^+_4$	0.00	3.99	0.01	1.98	0.01	0.01	0.01	0.00
16^+_1	99.5	$(p^4)^+_{12}(n^2)^+_4$	0.00	3.99	0.01	1.98	0.00	0.01	0.01	0.00
17^+_1	81	$(p^4)^-_{10}(n^2)^-_7$	0.86	2.99	0.15	1.12	0.00	0.01	0.00	0.86
18^+_1	99	$(p^4)^-_{11}(n^2)^-_7$	1.00	2.99	0.01	0.98	0.00	0.01	0.00	1.00
19^+_1	99.8	$(p^4)^-_{11}(n^2)^-_8$	1.00	2.98	0.02	1.00	0.00	0.00	0.00	1.00

considerably to the high-spin states. The $2n$ state with $J^{\pi} = 6^+$ is near 4 MeV in ^{90}Sr, as seen in Fig. 7. Around this excitation energy, $N = 50$ core excited states could appear.

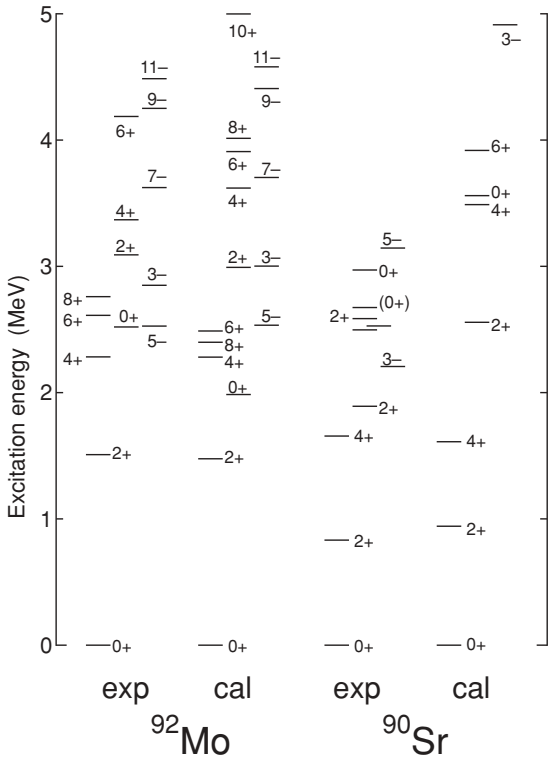

FIG. 7. Calculated energy levels of $4p$ and $2n$ subsystems, which are compared with energy levels observed in ^{92}Mo and ^{90}Sr.

Such configurations probably mix into the high-spin states in ^{94}Mo.

In Fig. 6(b), calculated energy levels with negative parity are compared with those observed in the present experiment. Our shell model reproduces well the observed level scheme, except that the 3^-_1 state lies above the 5^-_1 state in the calculation. It is difficult to get the correct order of the 3^-_1 and 5^-_1 states by changing the strengths of the octupole-octupole force within the present model space. The discrepancy is attributed to the insufficiency of the model space, in which only the $p_{1/2}$ orbital of the fp shell is included for protons. The 3^-_1 state must contain combinations of many particle-hole configurations. The 3^-_1 state, however, is not detected in the present experiment, which suggests a rather weak $5^-_1 \to 3^-_1$ transition. Our calculation gives the value $B(E2; 5^-_1 \to 3^-_1) =$ 1.2 W.u. Above the 3^-_1 state, on the contrary, calculated $B(E2; J^-_1 \to (J-2)^-_1)$ values are larger, i.e., 26.0, 28.2, 14.0, 12.8, and 9.6 W.u. respectively for $J = 7, 9, \ldots 15$. This prediction corresponds well to the observed cascade decay from (15^-_1) to (5^-_1). Above the 15^-_1 state, the $B(E2)$ values are very small except for $B(E2; 18^-_1 \to 16^-_1) = 1.03$ W.u. Our truncated model space seems to be insufficient also for negative-parity high-spin states. In any case, the present shell model is considered to be basically good for the yrast states and to provide information about the high-spin states. Let us look at their wave functions in Table IV.

Table IV indicates that the collective $5^-_1, 7^-_1, \ldots 15^-_1$ states are combinations of the product states of negative-parity proton basis states and positive-parity neutron basis states. It seems that mainly the four protons (one being in the $p_{1/2}$ orbital) bear high spin and the $2n$ basis states $(n^2)^+_{J=0}$, $(n^2)^+_{J=2}$, and $(n^2)^+_{J=4}$ assist. The variation of structure with increasing total

TABLE IV. Structure of negative-parity states in ^{94}Mo, tabulated in the same manner as Table III.

J_i^π	Leading config.		Proton $\langle n_a\rangle_p$			Neutron $\langle n_a\rangle_n$				
	%	$(p^4)^\pi_{Jp}(n^2)^\pi_{Jn}$	$p_{1/2}$	$g_{9/2}$	$d_{5/2}$	$d_{5/2}$	$s_{1/2}$	$d_{3/2}$	$g_{7/2}$	$h_{11/2}$
3^-_1	60	$(p^4)^-_3(n^2)^+_0$	1.00	2.79	0.13	1.72	0.15	0.07	0.05	0.01
5^-_1	78	$(p^4)^-_5(n^2)^+_0$	1.00	2.87	0.13	1.70	0.15	0.08	0.06	0.01
7^-_1	53	$(p^4)^-_5(n^2)^+_2$	1.00	2.87	0.13	1.69	0.19	0.07	0.04	0.01
9^-_1	43	$(p^4)^-_5(n^2)^+_4$	1.00	2.89	0.12	1.79	0.12	0.05	0.03	0.01
11^-_1	70	$(p^4)^-_{11}(n^2)^+_0$	1.00	2.95	0.05	1.71	0.15	0.07	0.06	0.01
13^-_1	75	$(p^4)^-_{11}(n^2)^+_2$	1.00	2.96	0.04	1.76	0.16	0.05	0.02	0.01
15^-_1	99	$(p^4)^-_{11}(n^2)^+_4$	1.00	2.99	0.01	1.97	0.00	0.02	0.00	0.01
14^-_1	99	$(p^4)^-_{10}(n^2)^+_4$	1.00	2.99	0.01	1.97	0.00	0.02	0.00	0.01
15^-_2	94	$(p^4)^+_8(n^2)^-_7$	1.83	2.12	0.06	1.04	0.00	0.01	0.00	0.95
16^-_1	99.5	$(p^4)^+_8(n^2)^-_8$	1.86	2.13	0.01	1.00	0.00	0.00	0.00	1.00
17^-_1	99.5	$(p^4)^-_{11}(n^2)^+_6$	1.00	2.99	0.02	0.99	0.00	0.00	1.00	0.01
17^-_2	94	$(p^4)^+_8(n^2)^-_9$	1.83	2.12	0.06	0.06	0.00	0.00	1.00	0.94
18^-_1	86	$(p^4)^+_{10}(n^2)^-_8$	0.00	3.93	0.07	0.96	0.04	0.00	0.00	1.00
19^-_1	99.8	$(p^4)^+_{12}(n^2)^-_7$	0.00	3.98	0.02	0.99	0.00	0.01	0.00	1.00

spin is similar to that for the positive-parity states in Table III. The 17^-_1 state is constructed by changing the $2n$ configuration, i.e., by 1 neutron jumping into the $g_{7/2}$ orbital. Other high-spin states get high spin by 1 neutron jumping into the $h_{11/2}$ orbital. We should expect admixture of additional configurations both for protons and neutrons, when we allow nucleon excitations from the $Z = 38$, $N = 50$ core.

The experiment observed some transitions from the negative-parity states to positive-parity states. Our truncated model space cannot give nonzero matrix elements for the $E1$ transition operator. (The model space, however, does not admix spurious components due to translation of the center of mass.) Instead we calculated $E3$ transition probabilities. The obtained $B(E3)$ values are much smaller ($<70\,e^2$ fm^6) than the Weisskopf unit 525 e^2 fm^6 for ^{94}Mo.

C. Structure of ^{95}Mo

We have carried out calculations for ^{95}Mo using the same parameters as for ^{94}Mo. Figure 8 shows calculated energy levels in comparison with experimental ones. Figure 8(a) shows a whole level scheme and Fig. 8(b) shows details of the low-energy part below 3 MeV. Some of the experimental data are taken from the ENSDF [23].

Our shell model reproduces well the observed energy levels below 3 MeV for an odd-mass nucleus. The $7/2^+_1$ and $11/2^+_1$ states are a little ($\sim$0.5 MeV) higher than the experimentally observed energies. Still, there is a reasonable correspondence between theory and experiment. Including the low-spin states ($1/2^+$–$7/2^+$) [23] in the left-most column, all the observed states below 3 MeV are reproduced in the calculation. The order of yrast states built on the ground state $5/2^+_1$ agrees with experiment except for the $7/2^+_1$ and $11/2^+_1$ states. Up to the $21/2^+_1$ state, the calculated $B(E2)$ values are rather in harmony with the observed decay scheme neglecting the problem for the $7/2^+_1$ and $11/2^+_1$ states. The shell-model calculation supports the level scheme obtained in the present experiment, which differs significantly from the previous ones [4,9]. Probably, there are no $5/2^+$ and $7/2^+$ states below the $7/2^+$ state at 0.77 MeV except for the ground state, and the state at 1.55 MeV is the $9/2^+_2$ state. It is most probable that the state at 2.77 MeV is the $21/2^+_1$ state. We may consider the decay scheme based on these suppositions.

The deviations of the $7/2^+_1$ and $11/2^+_1$ states from the observed positions, however, raise a question about the applicability of our model at low energy for ^{95}Mo. We first consider this question and assess to what extent our model describes the low-energy structure of ^{95}Mo. We analyze the details of wave functions that are given by the NuShellX code. Outlines are shown in Table V in the same way as in Tables III and IV.

The $5/2^+_1$ ground state has the leading configuration $(p^4)^+_0(n^3)^+_{5/2}$. The $3/2^+_1$ and $9/2^+_1$ states have also the leading configuration $(p^4)^+_0(n^3)^+_{3/2}$ and $(p^4)^+_0(n^3)^+_{9/2}$, although their squared amplitudes are not large enough. These three-neutron states $(n^3)^+_{J=5/2,3/2,9/2}$ have the leading component $(d_{5/2})^3_{J=5/2,3/2,9/2}$. The state $(d_{5/2})^3_{J=5/2}$ is a seniority $v = 1$ state and the states $(d_{5/2})^3_{J=3/2,9/2}$ are seniority $v = 3$ states. It is, however, known that $(d_{5/2})^3_{J=5/2}$ has the component $[(d_{5/2})^2_{J=0}d_{5/2}]_{J=5/2}$ only 22% (the squared cfp $\langle d_{5/2}(d_{5/2})^2_{J=5/2}]\}(d_{5/2})^3_{J=5/2}\rangle^2$ is 2/9). The $J = 0$ pairing interaction contributes little to the energy of the seniority $v = 1$ state $(d_{5/2})^3_{J=5/2}$. The $J = 2$ interaction also contributes to $(d_{5/2})^3_{J=5/2}$ less than to $(d_{5/2})^3_{J=3/2}$. This is the reason why the $5/2^+_1$ state is not so much lower than the $3/2^+_1$ state. Furthermore, Table V indicates that the three-neutron state $(n^3)^+_{5/2}$ has many other neutron configurations occupying the orbitals above $d_{5/2}$. Thus the lowest states $5/2^+_1$, $3/2^+_1$, and $9/2^+_1$ of ^{95}Mo are not the states with simple single-particle nature but have complicated configurations, in contrast with

TABLE V. Structure of positive- and negative-parity states in ^{95}Mo, tabulated in the same manner as Table III.

J_i^π	Leading config.		Proton $\langle n_a \rangle_p$			Neutron $\langle n_a \rangle_n$				
	%	$(p^4)^\pi_{Jp}(n^3)^\pi_{Jn}$	$p_{1/2}$	$g_{9/2}$	$d_{5/2}$	$d_{5/2}$	$s_{1/2}$	$d_{3/2}$	$g_{7/2}$	$h_{11/2}$
$1/2^+_1$	50	$(p^4)^+_0(n^3)^+_{1/2}$	1.69	2.21	0.10	2.17	0.59	0.17	0.06	0.01
$3/2^+_1$	41	$(p^4)^+_0(n^3)^+_{3/2}$	1.58	2.28	0.15	2.63	0.23	0.09	0.04	0.01
$5/2^+_1$	84	$(p^4)^+_0(n^3)^+_{5/2}$	1.61	2.26	0.13	2.72	0.12	0.08	0.06	0.01
$7/2^+_1$	34	$(p^4)^+_0(n^3)^+_{7/2}$	1.53	2.31	0.17	2.37	0.38	0.17	0.06	0.02
$9/2^+_1$	58	$(p^4)^+_0(n^3)^+_{9/2}$	1.66	2.22	0.12	2.81	0.08	0.06	0.04	0.01
$11/2^+_1$	28	$(p^4)^+_6(n^3)^+_{3/2}$	1.82	2.07	0.11	2.60	0.23	0.11	0.05	0.02
$13/2^+_1$	27	$(p^4)^+_6(n^3)^+_{3/2}$	1.86	2.06	0.08	2.69	0.16	0.08	0.05	0.01
$15/2^+_1$	44	$(p^4)^+_8(n^3)^+_{3/2}$	1.83	2.10	0.07	2.66	0.20	0.08	0.05	0.01
$17/2^+_1$	55	$(p^4)^+_8(n^3)^+_{3/2}$	1.82	2.13	0.06	2.65	0.21	0.08	0.05	0.01
$19/2^+_1$	61	$(p^4)^+_8(n^3)^+_{5/2}$	1.83	2.13	0.03	2.74	0.13	0.07	0.05	0.02
$21/2^+_1$	90	$(p^4)^+_8(n^3)^+_{5/2}$	1.79	2.18	0.03	2.73	0.10	0.08	0.06	0.02
$23/2^+_1$	91	$(p^4)^+_8(n^3)^+_{9/2}$	1.81	2.17	0.02	2.83	0.08	0.04	0.03	0.02
$25/2^+_1$	98	$(p^4)^+_8(n^3)^+_{9/2}$	1.80	2.18	0.02	2.86	0.05	0.04	0.03	0.02
$25/2^+_2$	56	$(p^4)^+_{10}(n^3)^+_{5/2}$	0.11	3.80	0.10	2.73	0.12	0.08	0.06	0.01
$27/2^+_1$	88	$(p^4)^+_8(n^3)^+_{11/2}$	1.78	2.19	0.03	1.82	0.15	0.27	0.75	0.01
$27/2^+_2$	53	$(p^4)^+_{12}(n^3)^+_{5/2}$	0.06	3.88	0.06	2.61	0.18	0.11	0.08	0.01
$29/2^+_1$	70	$(p^4)^+_{12}(n^3)^+_{5/2}$	0.01	3.95	0.05	2.75	0.09	0.07	0.07	0.01
$29/2^+_2$	64	$(p^4)^+_8(n^3)^+_{13/2}$	1.82	2.17	0.01	1.93	0.06	0.01	1.00	0.01
$31/2^+_1$	99	$(p^4)^+_8(n^3)^+_{15/2}$	1.84	2.15	0.01	1.97	0.00	0.02	1.00	0.01
$31/2^+_2$	90	$(p^4)^+_{12}(n^3)^+_{9/2}$	0.00	3.97	0.02	2.82	0.06	0.06	0.05	0.01
$7/2^-_2$	48	$(p^4)^-_4(n^3)^+_{3/2}$	1.00	2.84	0.16	2.73	0.12	0.08	0.06	0.01
$9/2^-_2$	45	$(p^4)^-_5(n^3)^+_{3/2}$	1.00	2.84	0.17	2.63	0.22	0.10	0.05	0.01
$11/2^-_1$	64	$(p^4)^-_5(n^3)^+_{3/2}$	1.00	2.83	0.17	2.58	0.26	0.10	0.05	0.01
$13/2^-_1$	39	$(p^4)^-_5(n^3)^+_{5/2}$	0.99	2.86	0.15	2.65	0.19	0.09	0.05	0.01
$15/2^-_1$	76	$(p^4)^-_5(n^3)^+_{5/2}$	0.99	2.87	0.14	2.69	0.14	0.09	0.06	0.02
$17/2^-_1$	37	$(p^4)^-_5(n^3)^+_{5/2}$	0.99	2.87	0.14	2.57	0.24	0.11	0.06	0.02
$19/2^-_1$	47	$(p^4)^-_7(n^3)^+_{5/2}$	0.99	2.88	0.13	2.72	0.13	0.08	0.05	0.02
$21/2^-_1$	35	$(p^4)^-_9(n^3)^+_{5/2}$	0.99	2.90	0.10	2.60	0.22	0.11	0.05	0.02
$23/2^-_1$	51	$(p^4)^-_9(n^3)^+_{5/2}$	0.99	2.92	0.09	2.67	0.17	0.09	0.06	0.02
$25/2^-_1$	59	$(p^4)^-_{11}(n^3)^+_{5/2}$	0.99	2.96	0.05	2.71	0.14	0.08	0.05	0.02
$27/2^-_1$	85	$(p^4)^-_{11}(n^3)^+_{5/2}$	0.99	2.97	0.04	2.73	0.10	0.08	0.07	0.02
$29/2^-_1$	88	$(p^4)^-_{11}(n^3)^+_{9/2}$	0.99	2.98	0.03	2.83	0.08	0.04	0.03	0.02
$31/2^-_1$	98	$(p^4)^-_{11}(n^3)^+_{9/2}$	0.99	2.99	0.02	2.85	0.05	0.04	0.03	0.02
$35/2^-_1$	99	$(p^4)^+_8(n^3)^-_{19/2}$	1.85	2.14	0.01	1.95	0.00	0.03	0.01	1.01
$37/2^-_1$	99	$(p^4)^-_{11}(n^3)^+_{15/2}$	0.99	2.98	0.02	1.97	0.00	0.01	1.00	1.01
$39/2^-_1$	99	$(p^4)^+_8(n^3)^-_{23/2}$	1.85	2.14	0.01	1.00	0.00	0.00	0.99	1.00

the $1/2^+_1$ state that has a considerable single-particle nature as seen in Table V.

The $7/2^+_1$ state does not have single-particle nature in our calculation, but its low energy is rather well reproduced. Having the $g_{7/2}$ orbital at relatively high energy can be appropriate as mentioned in the previous subsection. However, the experimental low energy demands additional effects to lower the $7/2^+_1$ state. One nucleon transfer reactions [24] find a large component of one $g_{7/2}$ nucleon for the $7/2^+_1$ state. There remains a problem for the spectroscopic factor in our treatment. A mechanism for much more admixing of the $g_{7/2}$ orbital may be necessary. There is another possibility for $g_{9/2}$ contribution that is not included in our model space. Remember that the $(d_{5/2})^3$ configuration does not give spin $J = 7/2$. This is a reason why the $7/2^+_1$ energy is relatively high as compared with the $9/2^+_1$ state in the calculation. The effects of a $g_{9/2}$ neutron excitation are considered to be weak for the $5/2^+_1$, $3/2^+_1$, and $9/2^+_1$ states, because the additional configurations have more or less higher energy than the leading configuration $(d_{5/2})^3_J$ and hence give only small perturbations. In contrast, the effects are probably large for the $7/2^+_1$ state without the configuration $(d_{5/2})^3_{J=7/2}$. Note that the QQ matrix

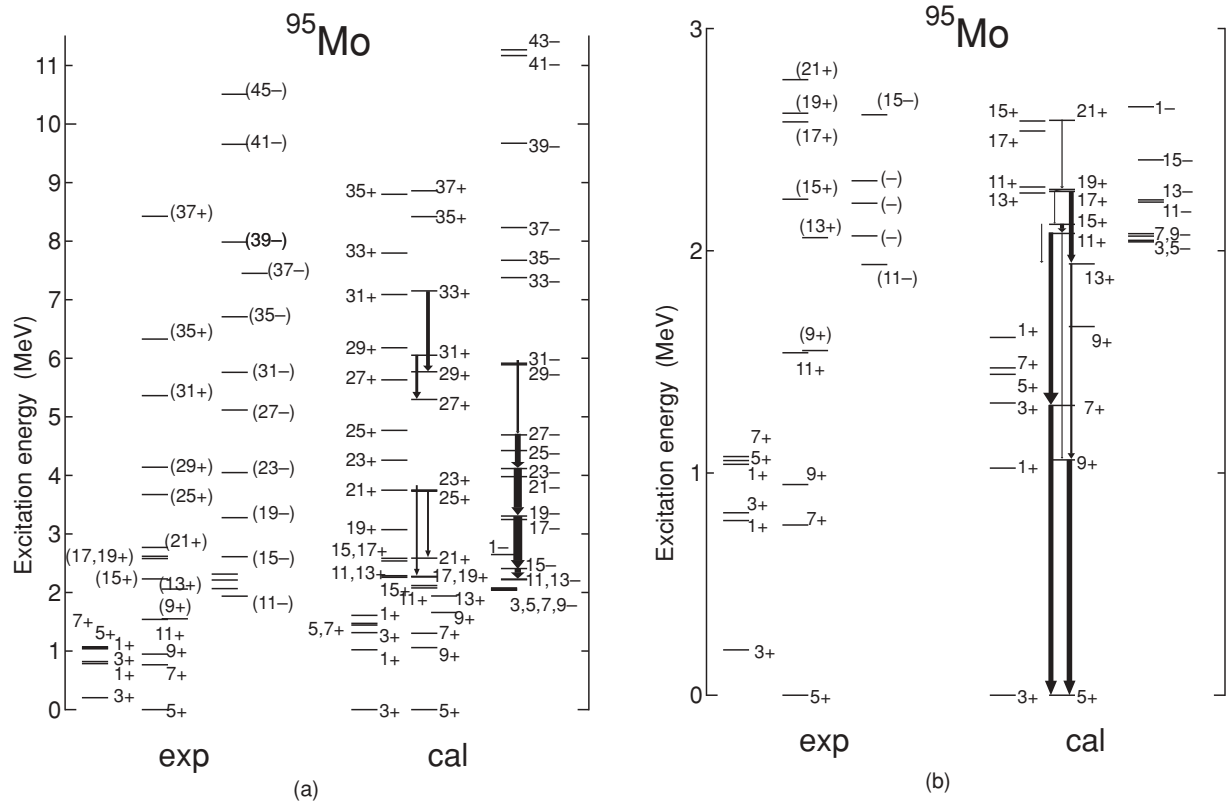

FIG. 8. Calculated energy levels of ^{95}Mo, which are compared with experimental ones. The spin of each state is denoted by the double number $2J$. The widths of the arrows denote relative values of $B(E2)$.

element of the $g_{9/2}$ orbital with the $d_{5/2}$ orbital is the largest. The experiment demands additional effects to lower the $11/2^+_1$ state also. The $g_{9/2}$ neutron excitation may cause the effects. We can say that our model is capable of describing the structure of low-lying states although it has a defect for the $7/2^+_1$ and $11/2^+_1$ states.

The observed values of $B(E2; 3/2^+_1 \to 5/2^+_1) = 21.5(11)$ W.u. and $B(E2; 9/2^+_1 \to 5/2^+_1) = 11.3(6)$ W.u. indicate the collective nature of these states, which is consistent with our results mentioned above. The calculation using the effective charges $e_p = 2.1e$ and $e_n = 1.0e$, however, gives too large values 34.9 and 17.9 in W.u. for these transitions. We need to use smaller effective charges to reproduce the observed $B(E2)$ values. This may suggest less excitation of "the core" in ^{95}Mo than in ^{94}Mo. Using the effective charges $e_p = 1.75e$ and $e_n = 0.75e$, we get good values $B(E2; 3/2^+_1 \to 5/2^+_1) = 21.9$ W.u. and $B(E2; 9/2^+_1 \to 5/2^+_1) = 11.5$ W.u. For $B(E2; 1/2^+_1 \to 3/2^+_1)$, we have also a good correspondence between the experimental value 3.9 W.u. and calculated value 3.7 W.u. However, our shell model fails to explain the small $B(E2)$ values for the transitions $7/2^+_1 \to 3/2^+_1$ and $7/2^+_1 \to 5/2^+_1$: the calculated values 7.7 and 10.5 W.u. deviate much from the observed ones of 0.012 and 0.96 W.u., respectively. Our model does not describe well the wave function of the $7/2^+_1$ state as mentioned above.

Table V gives the following information about high-spin states: above the $11/2^+_1$ state, high spin is supplied mainly by the two protons in the $g_{9/2}$ orbital coupled with the lowest three-neutron states; for $J \geqslant 25/2$, the states with four protons in the $g_{9/2}$ orbital and states with one neutron in the $g_{7/2}$ orbital compete with each other. It is likely that a neutron excitation from the $g_{9/2}$ orbital disturbs these states. The $B(E2)$ values larger than 1 W.u. are illustrated with the widths of arrows for positive-parity high-spin states in Fig. 8(a). A relatively large value $B(E2; 25/^+_1 \to 21/2^+_1) = 3.9$ W.u. corresponds to the observed decay $25/^+_1 \to 21/2^+_1$. The present shell model, however, is not sufficiently good for discussing the observed decay scheme for positive-parity high-spin states above $25/2^+_1$. The calculation shows also that there are other excited states near the yrast state of each J. We can say that a few decay bands could be detected in future experiments.

Last, let us consider negative-parity states. Experimentally observed states near the $(11/2^-_1)$ state at 1.94 MeV, spins of which have not been assigned, are probably the low-spin states with spins $3/2^-$ to $9/2^-$ in addition to the $13/2^-_1$ state. Our calculation reproduces the states $11/2^-_1$, $15/2^-_1$, $19/2^-_1$, $23/2^-_1$, $27/2^-_1$, and $31/2^-_1$ at good positions near the corresponding observed levels and gives large $E2$ transition probabilities for the $\Delta J = 2$ cascade decay to the $11/2^-_1$ state. Calculated $B[E2; J^-_1 \to (J-2)^-_1]$ values are 5.1, 12.1, 16.9, 18.5, and 13.1 W.u. for the transitions $31/2^-_1 \to 27/2^-_1 \to 23/2^-_1 \to 19/2^-_1 \to 15/2^-_1 \to 11/2^-_1$. Therefore, the present model can be considered to describe fairly well the states up to $31/2^-_1$. The calculation gives large $E2$ transition probabilities for another $\Delta J = 2$ cascade decay to the $13/2^-_1$

state. Calculated $B[E2; J_1^- \rightarrow (J-2)_1^-]$ values are 3.2, 12.8, 17.2, and 18.6 W.u. for the transitions $29/2_1^- \rightarrow 25/2_1^- \rightarrow 21/2_1^- \rightarrow 17/2_1^- \rightarrow 13/2_1^-$. This suggests that another cascade band on the $13/2_1^-$ state could be detected. The calculation predicts nearly degenerate $11/2_1^-$ and $13/2_1^-$ states and a large $B(E2; 15/2_1^- \rightarrow 13/2_1^-)$ value of 7.9 W.u. This could make the decay scheme complicated. Table V indicates that the negative-parity states up to $31/2_1^-$ contain three protons in the upper orbitals $(g_{9/2}, d_{5/2})$ and 1 proton in the $p_{1/2}$ orbital coupled mainly to the lowest states $(5/2_1^+, 3/2_1^+ 9/2_1^+)$ of three neutrons. We can suppose that these states are less affected by neutron excitation from the $g_{9/2}$ orbital.

Our model may not be powerful enough for discussing the correspondence between the experimental and calculated states above the $31/2_1^-$ state. The calculation has the $45/2_1^-$ state at much higher energy (12.8 MeV) compared with the $(45/2^-)$ level observed at 10.5 MeV.

V. SUMMARY

This article presents the results of an in-beam study of high-spin states in ^{94,95}Mo populated through the ^{16}O(^{82}Se, $xn\gamma$)^{94,95}Mo($x = 4, 3$) reactions. With the help of the high detection sensitivity of the GASP multidetector array and double-gating techniques, much revised level schemes of ^{94}Mo and ^{95}Mo have been constructed. Both positive- and negative-parity level sequences have been established in these two nuclei. The identification of crossover and doublet transitions provides many checks for the multipolarity, placement, and ordering of transitions in the present level schemes.

We have carried out shell-model calculations for ^{94,95}Mo in the model space of $\pi(p_{1/2}, g_{9/2}, d_{5/2})^4$ and $\nu(d_{5/2}, s_{1/2}, d_{3/2}, g_{7/2}, h_{11/2})^{2(3)}$. A parameter set of the extended $P + QQ$ interaction was determined for the $40 \leqslant Z \leqslant 42$ and $50 \leqslant N \leqslant 53$ nuclei including ^{94,95}Mo. The shell model explains satisfactorily the overall level schemes observed in these nuclei. For ^{94,95}Mo, the calculated results are in agreement with the experimental results.

Based on the fairly good agreement, we have discussed the structure of ^{94,95}Mo. The shell-model results show that the yrast states up to 12_1^+ and 15_1^- in ^{94}Mo and those up to $25/2_1^+$ and $31/2_1^-$ in ^{95}Mo can be explained in terms of the product space of the $4p$ states $(p_{1/2}, g_{9/2}, d_{5/2})^4$ and $2n$ $(3n)$ states $(d_{5/2}, s_{1/2}, d_{3/2}, g_{7/2}, h_{11/2})^{2(3)}$. From the calculated wave functions, most of these states are not simple single-particle states but are considerably collective as suggested by the observed $B(E2)$ values of more than 10 W.u.

The excitation energies of higher-spin states are also basically reproduced within the present model space. However, the deviations of the calculated energies from the experimental ones indicate a possible contribution from the $Z = 38$, $N = 50$ core, especially neutron excitations from the $g_{9/2}$ orbital. If we compare the excitation energies of the high-spin states with the shell gaps of the $Z = 38$, $N = 50$ core, probably the core excitations have effects on the high-spin states. The calculated $B(E2)$ values for the high-spin states are much smaller than those for the low-spin states. This is not in harmony with the observation of the cascade decay, and the core excitations should be included as the spin J increases.

ACKNOWLEDGMENTS

We thank the technical staff of the TANDEM-ALPI accelerator complex of the Laboratori Nazionali di Legnaro for their support during the experiment. Many thanks are due to the GASP group for running the apparatus. This work has been supported in part by the EU (contract no. ERBFMGECT 980110), the CAS, the NSFC, and the Major State Basic Research Development Program of China (2007CB815005,10735010). One of the authors, G. de A. was partially supported by the Alexander von Humbold Foundation. M.H. is grateful to Professor X. H. Zhou and other members of Institute of Modern Physics, Chinese Academy of Sciences, for their hospitality. He acknowledges useful discussions with Professors Y. Sun, K. Kaneko, and T. Mizusaki.

[1] Xiandong Ji and B. H. Wildenthal, Phys. Rev. C **37**, 1256 (1988).
[2] S. S. Ghugre and S. K. Datta, Phys. Rev. C **52**, 1881 (1995).
[3] B. Kharraja, S. S. Ghugre, U. Garg, R. V. F. Janssens, M. P. Carpenter, B. Crowell, T. L. Khoo, T. Lauritsen, D. Nisius, W. Reviol, W. F. Mueller, L. L. Riedinger, and R. Kaczarowski, Phys. Rev. C **57**, 83 (1998).
[4] B. Kharraja, S. S. Ghugre, U. Garg, R. V. F. Janssens, M. P. Carpenter, B. Crowell, T. L. Khoo, T. Lauritsen, D. Nisius, W. Reviol, W. F. Mueller, L. L. Riedinger, and R. Kaczarowski, Phys. Rev. C **57**, 2903 (1998).
[5] C. M. Lederer, J. M. Jaklevic, and J. M. Hollander, Nucl. Phys. **A169**, 449 (1971).
[6] C. M. Lederer, J. M. Jaklevic, and J. M. Hollander, Nucl. Phys. **A169**, 489 (1971).
[7] L. Mesko, A. Nilsson, S. A. Hjorth, M. Brenner, and O. Holmlund, Nucl. Phys. **A181**, 566 (1972).
[8] D. Bazzacco, Proceeding of the International Conference on Nuclear Structure at High Angular Momentum, Ottawa 1992, Report No. AECL 10613 (unpublished), Vol. 2, p. 376.
[9] J. M. Chatterjee, M. Saha-Sarkar, S. Bhattacharya, S. Sarkar, R. P. Singh, S. Murulithar, and R. K. Bhowmik, Phys. Rev. C **69**, 044303 (2004).
[10] Y. H. Zhang, Zs. Podolyak, G. de Angelis, A. Gadea, C. Ur, S. Lunardi, N. Marginean, C. Rusu, R. Schwengner, Th. Kroll, D. R. Napoli, R. Menegazzo, D. Bazzacco, E. Farnea, S. Lenzi, T. Martinez, M. Axiotis, D. Tonev, W. Gelletly, S. Langdown, P. H. Regan, J. J. Valiente-Dobon, W. von Oertzen, B. Rubio, B. Quintana, N. Medina, R. Broda, D. Bucurescu, M. Ionescu-Bujor, and A. Iordachescu, Phys. Rev. C **70**, 024301 (2004).
[11] G. A. Jones, Zs. Podolyak, N. Schunck, P. M. Walker, G. De Angelis, Y. H. Zhang, M. Axiotis, D. Bazzacco, P. G. Bizzeti, F. Brandolini, R. Broda, D. Bucurescu, E. Farnea, W. Gelletly, A. Gadea, M. Ionescu-Bujor, A. Iordachescu, Th. Kroll, S. D. Langdown, S. Lunardi, N. Marginean, T. Martinez,

N. H. Medina, B. Quintana, P. H. Regan, B. Rubio, C. A. Ur, J. J. Valiente-Dobon, and S. J. Williams, Acta Phys. Pol. B **36**, 1323 (2005).
[12] J. B. Moorhead and R. A. Moyer, Phys. Rev. **184**, 1205 (1969).
[13] D. Bucurescu, Che. Căta-Danil, I. Căta-Danil, M. Ivaşcu, N. Mărginean, and C. A. Ur, Phys. Rev. C **63**, 014306 (2000).
[14] M. Hasegawa and K. Kaneko, Phys. Rev. C **59**, 1449 (1999).
[15] M. Hasegawa, K. Kaneko, and S. Tazaki, Nucl. Phys. **A674**, 411 (2000); **688**, 765 (2001); Prog. Theor. Phys. **107**, 731 (2002).
[16] A. Saganek, V. Meyer, S. Mirowski, M. Oteski, M. Sieme'aski, E. Wesolowski, and Z. Wilhelm, J. Phys. G **10**, 549 (1984).
[17] T. P. Clearly, Nucl. Phys. **A301**, 317 (1978).
[18] A. Holt, T. Engeland, M. Hjorth-Jensen, and E. Osnes, Phys. Rev. C **61**, 064318 (2000).
[19] C. O''zen and D. J. Dean, Phys. Rev. C **73**, 014302 (2006).
[20] M. Hasegawa, K. Kaneko, T. Mizusaki, and S. Tazaki, Phys. Rev. C **69**, 034324 (2004).
[21] K. Kaneko, Y. Sun, M. Hasegawa, and T. Mizusaki, Phys. Rev. C **77**, 064304 (2008); [Erratum-*ibid.* **78**, 049903 (2008)].
[22] W. Rae, the article and the NuShellX code on the Web site http://knollhouse.org., released in 2008.
[23] http://www.nndc.bnl.gov/ensdf/.
[24] S. A. Sultana, D. Maki, G. Wakabayashi, Y. Uozumi, N. Ikeda, Syafarudin, F. Aramaki, T. Kawaguchi, M. Matoba, and H. M. Sen Gupta Phys. Rev. C **70**, 034612 (2004).